

Manifold-Constrained MPPI: Real-Time Sampling-Based Control Under Hard Constraints

Seulchan Lee, Sanghyun Kim

Abstract—Sampling-based model predictive control methods, such as Model Predictive Path Integral (MPPI), offer derivative-free optimization and robustness in complex robotic systems. However, standard MPPI relies on cost-based soft penalties that cannot guarantee hard-constraint satisfaction, severely limiting its applicability to highly constrained tasks such as closed-chain manipulation. To address this, we propose Manifold-Constrained MPPI (MC-MPPI), a real-time sampling-based control framework that enforces manifold-based equality constraints while preserving the computational advantages of MPPI. The key idea is to decouple the constrained optimal control problem into latent-space planning and execution-level correction. At the planning stage, a Variational Autoencoder (VAE) learns a low-dimensional latent representation of the constraint manifold, enabling MPPI to efficiently generate near-feasible candidate trajectories without per-sample modification. Since this reference enables accurate linearization of the equality constraints, an execution-level Quadratic Programming (QP) controller resolves the residual manifold mismatch in a single solve rather than through iterative projection. Experiments on a 14-DoF closed-chain dual-arm system in both simulation and real-world settings demonstrate that MC-MPPI operates stably at 100 Hz, reliably navigates dynamic environments while effectively maintaining hard equality constraints, and significantly outperforms baseline methods in tracking accuracy. Supplementary videos and implementation details are available at <https://rcilab.github.io/mcmpi>.

Index Terms—optimal control, constrained sampling, constrained manipulation, model predictive path integral

I. INTRODUCTION

Robotic systems subject to strict kinematic constraints—such as the closed-chain dual-arm manipulation task [1]—require controllers that maintain constraint satisfaction in real time. Even marginal violations of these constraints can result in excessive internal forces, object damage, or complete loss of grasp stability. Enforcing kinematic constraints in robotic manipulation has been widely addressed through model predictive control with gradient-based solvers such as SQP [2], [3], DDP [4], [5], and iLQR [6], which directly handle nonlinear constraint satisfaction. While mathematically rigorous, these approaches share common limitations: sensitivity to local minima in non-convex optimization problems and computational costs that scale poorly with the number of constraints and planning horizon. Moreover, they operate directly in the full configuration space, where the feasible set occupies a thin, nonlinear submanifold.

Seulchan Lee and Sanghyun Kim are with the School of Mechanical Engineering, Kyung Hee University, Yongin, South Korea (e-mail: {lee081847, kim87}@khu.ac.kr). Sanghyun Kim is also with the Advanced Institute of Convergence Technology, Suwon, South Korea.

*Corresponding author: Sanghyun Kim.

Model Predictive Path Integral (MPPI) [7], [8] control, a highly effective sampling-based framework for complex robotic systems, offers an alternative paradigm by replacing gradient-based optimization with a derivative-free approach that is inherently robust to local minima. Leveraging recent advancements in GPU hardware, Bhardwaj *et al.* [9] introduced the STORM framework, which demonstrated that MPPI scales effectively to high-dimensional, redundant manipulators, enabling real-time trajectory optimization with thousands of parallel rollouts. Yet a fundamental limitation remains: standard MPPI relies on cost-based soft penalties to handle constraints, treating violations as additive cost terms rather than strict mathematical boundaries. This precludes any guarantee of hard-constraint satisfaction, critically limiting its applicability to tasks where physical feasibility must be maintained at all times.

To handle constraints within the MPPI framework, widely adopted approaches employ proactive safety filtering methodologies. A prominent direction utilizes Control Barrier Functions (CBFs) to delineate safe sets within the state space. For instance, to enforce safety-critical conditions such as obstacle avoidance, Ardiyanto *et al.* [10] addressed inequality constraints by formulating CBFs as soft penalties within the MPPI framework. Also, Shield-MPPI [11] introduces a discrete-time CBF-based penalty combined with a local gradient-based repair step. However, these approaches—whether relying on soft penalties or local repairs—commonly share a limitation in fully satisfying hard constraints. Consequently, such architectures may exhibit suboptimal safety behaviors, especially in highly constrained environments.

To incorporate constraint information directly into the sampling process, constraint-aware sampling strategies have emerged as a powerful alternative. Several recent approaches such as π -MPPI [12], SCP-MPPI [13], and CSC-MPPI [14] modify sampled control sequences through quadratic programming-based projections, Stein Variational Gradient Descent (SVGD), and iterative primal-dual updates based on Karush-Kuhn-Tucker (KKT) conditions, respectively. However, these state-of-the-art correction mechanisms are fundamentally designed to handle inequality constraints, such as safety boundaries or control limits. They are not directly applicable to manifold-based nonlinear equality constraints that define the feasible state space. Unlike inequality regions that allow for a range of feasible solutions, equality constraints confine the system to a lower-dimensional subspace with zero Lebesgue measure. Consequently, standard inequality-based filters often exhibit severe computational bottlenecks and numerical instability when enforcing high-dimensional samples to lie effectively on such complex geometric structures.

To address this challenge, this paper proposes Manifold-Constrained MPPI (MC-MPPI), a novel real-time control framework that effectively enforces manifold-based equality constraints. The key idea is to decouple constraint handling into planning and execution. Rather than correcting every sampled trajectory to satisfy the constraints, MC-MPPI plans in a learned latent representation and resolves the constraint mismatch only once for the selected solution at execution. At the planning stage, inspired by recent advances in using generative models to approximate complex task and kinematic constraints [15], [16], a Variational Autoencoder (VAE) [17] is employed to learn a continuous, lower-dimensional latent representation of the constraint manifold. Instead of sampling in the high-dimensional full configuration space—where nearly all samples would violate the zero-measure equality constraints—the framework samples directly in this structured latent space. This enables MPPI to efficiently generate thousands of candidate trajectories that are structurally near-feasible, while avoiding the prohibitive cost of modifying every individual sample. However, because a learned generative model inevitably introduces approximation errors, a manifold mismatch remains. To address this, at the execution stage, a QP-based optimal controller [18] is employed exclusively on the selected solution to resolve the residual manifold mismatch.

Therefore, the primary contributions of this study are summarized as follows:

- **A Manifold-Constrained MPPI Framework for Hard Constraints:** We propose MC-MPPI, a real-time sampling-based control framework that effectively enforces manifold-based equality constraints. By decoupling the constrained optimal control problem into latent-space planning and execution, the framework preserves the derivative-free, parallelizable advantages of MPPI while maintaining physical feasibility.
- **Computationally Efficient Resolution of Manifold Mismatch via Single-Step QP:** To resolve the manifold mismatch inherent in learned generative models, we introduce a computationally efficient two-stage architecture. Because the latent-space planning provides a structurally near-feasible reference, the nonlinear equality constraints can be accurately linearized. This enables the execution-level QP controller to eliminate residual errors in a single solve rather than through iterative manifold projection, maintaining stable real-time operation at high control frequency.
- **Experimental Validation in Simulation and on a Real Closed-Chain Dual-Arm Setup:** The proposed framework is validated through both simulation and hardware experiments. The results demonstrate that MC-MPPI achieves 100 Hz real-time control on the 14-DoF closed-chain dual-arm system, reliably navigating obstacle-rich environments while effectively maintaining manifold-based equality constraints.

II. REVIEW OF MPPI

For readability, we adopt the following notation conventions throughout this paper: $(\hat{\cdot})$, $(\dot{\cdot})^*$, and $(\cdot)^*$ denote perturbed,

near-feasible, and optimal quantities, respectively.

MPPI is a sampling-based optimal control framework that replaces gradient-based optimization with importance sampling over the control space. Consider a discrete-time stochastic nonlinear system:

$$\mathbf{x}_{t+1} = f(\mathbf{x}_t, \tilde{\mathbf{u}}_t), \quad (1)$$

where $\mathbf{x}_t \in \mathbb{R}^{n_s}$ is the state and $\tilde{\mathbf{u}}_t \in \mathbb{R}^{n_u}$ is the perturbed control input at time step t . The controller maintains a control sequence $\mathbf{U} = [\mathbf{u}_0, \dots, \mathbf{u}_{T-1}]$ over a finite horizon T , where each perturbed control is generated as:

$$\tilde{\mathbf{u}}_t = \mathbf{u}_t + \delta \mathbf{u}_t, \quad \delta \mathbf{u}_t \sim \mathcal{N}(\mathbf{0}, \Sigma), \quad (2)$$

where Σ is the exploration covariance matrix. For each sampled control trajectory $\tilde{\mathbf{U}} = [\tilde{\mathbf{u}}_0, \dots, \tilde{\mathbf{u}}_{T-1}]$, the state sequence, $\mathbf{X} = [\mathbf{x}_0, \dots, \mathbf{x}_T]$, is obtained by forward propagation through (1), and its performance is evaluated by the trajectory cost:

$$S(\mathbf{X}) = \phi(\mathbf{x}_T) + \sum_{t=0}^{T-1} c(\mathbf{x}_t), \quad (3)$$

where $\phi(\mathbf{x}_T)$ is the terminal cost and $c(\mathbf{x}_t)$ is the stage cost.

The objective is to find the optimal control sequence \mathbf{U}^* that minimizes $\mathbb{E}[S(\mathbf{X})]$, but a direct solution is intractable. By applying the free energy formulation and Jensen's inequality, the stochastic optimal control problem can be reformulated as minimizing the KL divergence between the optimal trajectory distribution \mathbb{Q}^* and the proposal distribution \mathbb{Q} [7]:

$$\mathbf{U}^* \simeq \arg \min_{\mathbf{U}} D_{\text{KL}}(\mathbb{Q}^* \parallel \mathbb{Q}), \quad (4)$$

whose solution yields:

$$\begin{aligned} \mathbf{U}^* &= \arg \min_{\mathbf{U}} \mathbb{E}_{\mathbb{Q}^*} \left[\frac{1}{2} \sum_{t=0}^{T-1} (\tilde{\mathbf{u}}_t - \mathbf{u}_t)^T \Sigma^{-1} (\tilde{\mathbf{u}}_t - \mathbf{u}_t) \right] \\ &= \mathbb{E}_{\mathbb{Q}^*} [\tilde{\mathbf{U}}], \end{aligned} \quad (5)$$

stating that the optimal control sequence is the expectation under \mathbb{Q}^* . Since sampling directly from \mathbb{Q}^* is intractable, importance sampling is applied to express the expectation under the proposal distribution \mathbb{Q} . The resulting importance weights are approximated via K Monte Carlo samples. For each sample $k \in \{1, \dots, K\}$, a perturbed control sequence is generated by instantiating (2) as:

$$\tilde{\mathbf{u}}_t^{(k)} = \mathbf{u}_t + \delta \mathbf{u}_t^{(k)}, \quad \delta \mathbf{u}_t^{(k)} \sim \mathcal{N}(\mathbf{0}, \Sigma), \quad (6)$$

and rolled out through (1) to obtain the trajectory cost $S^{(k)}$. Each sample is assigned the importance weight:

$$w^{(k)} = \frac{\exp(-\frac{1}{\lambda} S^{(k)})}{\sum_{j=1}^K \exp(-\frac{1}{\lambda} S^{(j)})}, \quad (7)$$

where $\lambda > 0$ is the temperature parameter. The optimal control sequence is computed as the importance-weighted average:

$$\mathbf{U}^* \leftarrow \sum_{k=1}^K w^{(k)} \tilde{\mathbf{U}}^{(k)}. \quad (8)$$

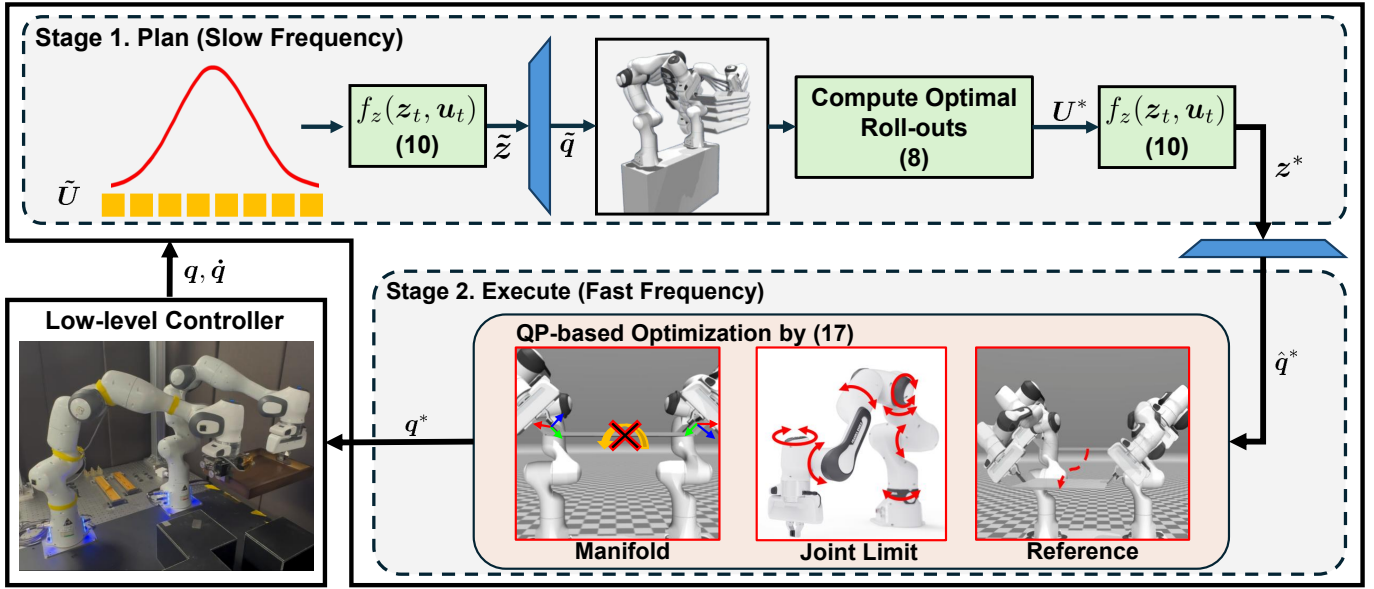


Fig. 1: Overall architecture of the MC-MPPI framework. The upper-level planner performs MPPI in a VAE-learned latent space to efficiently generate near-feasible candidate trajectories under manifold-based equality constraints. The decoded nominal solution is then corrected by a single-step QP to effectively satisfy the hard constraints, and the resulting reference is tracked by an optimization-based low-level controller. In our experiments with the dual-arm system, the slow-frequency planner operates at 100 Hz, while the fast-frequency executor runs at 500 Hz.

The first action u_0 is applied to the system, the horizon is shifted forward, and the process repeats in a receding-horizon fashion.

While standard MPPI efficiently handles non-convex cost landscapes through massively parallel sampling, it provides no mechanism to enforce hard constraints—violations are penalized through cost terms but never eliminated. This motivates the manifold-constrained formulation proposed in this work.

III. MC-MPPI FRAMEWORK

This section presents the proposed MC-MPPI framework, as illustrated in Fig. 1. The framework adopts a hierarchical control architecture consisting of an upper level planner and a lower level controller. The upper level planner performs latent-space sampling-based optimization to generate a near-feasible reference configuration, \hat{q}^* , at each control cycle, as described in Subsection III-A. The lower level execution module corrects the reference to effectively satisfy the hard constraints and tracks it via a low-level controller (a position controller in our implementation), as detailed in Subsection III-B.

A. Planning Stage

1) *Manifold Learning via VAE*: Consider an n -dimensional robotic system subject to l kinematic equality constraints defined by $h : \mathbb{R}^n \rightarrow \mathbb{R}^l$ with $h(q) = \mathbf{0}$, which induce a nonlinear constraint manifold

$$\mathcal{M} = \{q \in \mathbb{R}^n \mid h(q) = \mathbf{0}\}, \quad (9)$$

with intrinsic dimension $m = n - l$. Planning directly on \mathcal{M} is difficult because it is a lower-dimensional set embedded in \mathbb{R}^n , so naive sampling in the ambient space yields

feasible configurations with probability zero. To address this, a VAE is employed to learn a continuous, low-dimensional latent space that captures the structure of \mathcal{M} . The pre-trained decoder $\psi_\theta : \mathbb{R}^m \rightarrow \mathbb{R}^n$ then provides a nonlinear map that approximately parameterizes \mathcal{M} , enabling trajectory optimization to be performed in the unconstrained latent space while producing near-feasible configurations.

2) *Latent Space Control Formulation*: To perform manifold-constrained sampling within the MPPI framework, candidate trajectories must be generated in a space where feasible samples can be obtained efficiently. To this end, the proposed framework executes latent motion within the learned latent space \mathbb{R}^m of the VAE, rather than sampling directly in the ambient configuration space \mathbb{R}^n , where feasible configurations form a zero-measure subset under any continuous distribution.

To realize this latent motion, we consider stochastic latent-space dynamics analogous to (1). Here, $u_t \in \mathbb{R}^m$ denotes the latent control input, in contrast to the original control input in Section II, where $u_t \in \mathbb{R}^{n_u}$. Specifically, u_t is interpreted as the latent-space velocity \dot{z}_t , so that the latent evolution is modeled by the following first-order Euler integration:

$$z_{t+1} = f_z(z_t, \tilde{u}_t) = z_t + \tilde{u}_t \Delta t. \quad (10)$$

As in the standard MPPI formulation in (2), the actual latent control input is given by

$$\tilde{u}_t = u_t + \delta u_t, \quad \delta u_t \sim \mathcal{N}(\mathbf{0}, \Sigma). \quad (11)$$

Based on this formulation, the stochastic optimal control problem is defined over a horizon T with latent control

sequence $\mathbf{U} = [\mathbf{u}_0, \mathbf{u}_1, \dots, \mathbf{u}_{T-1}]^T \in \mathbb{R}^{T \times m}$ as

$$\begin{aligned} \min_{\mathbf{U}} J &= \mathbb{E} \left[\phi(\mathbf{z}_T) + \sum_{t=0}^{T-1} \left(c(\mathbf{z}_t) + \frac{1}{2} \mathbf{u}_t^T \mathbf{R} \mathbf{u}_t \right) \right], \\ \text{s.t. } \mathbf{z}_{t+1} &= \mathbf{z}_t + \tilde{\mathbf{u}}_t \Delta t, \\ \tilde{\mathbf{u}}_t &= \mathbf{u}_t + \delta \mathbf{u}_t, \quad \delta \mathbf{u}_t \sim \mathcal{N}(\mathbf{0}, \Sigma), \\ \mathbf{z}_0 &= \mathbf{z}_{\text{init}}, \end{aligned} \quad (12)$$

where $c(\mathbf{z}_t)$ and $\phi(\mathbf{z}_T)$ denote the stage and terminal costs, respectively, and $\mathbf{R} \succ 0$ is the control weight matrix.

3) *MPPI in Latent Space*: Since the optimization problem in (12) is formulated in the latent space, costs defined in the joint and operational spaces—such as end-effector tracking error, collision avoidance, and joint limits—cannot be evaluated directly from latent samples $\tilde{\mathbf{z}}$. Therefore, each predicted latent state along a sampled trajectory is decoded into the joint space using the pre-trained decoder:

$$\tilde{\mathbf{q}}_{t+1}^{(k)} = \psi_\theta(\tilde{\mathbf{z}}_{t+1}^{(k)}), \quad \forall t = 0, \dots, T-1 \quad (13)$$

where ψ_θ denotes the pre-trained decoder described in Subsection III-A1. The decoded trajectory $\tilde{\mathbf{q}}^{(k)}$ is then used to evaluate the trajectory cost $S^{(k)}$ in the joint and operational spaces, enabling meaningful cost comparison across all K sampled trajectories.

However, the quality of the decoded joint trajectory $\tilde{\mathbf{q}}^{(k)}$ is sensitive to the temporal continuity of the latent samples $\tilde{\mathbf{z}}^{(k)}$. To ensure smooth decoding while maintaining computational efficiency, we adopt the single-instance sampling strategy proposed in [19], which maintains a constant control innovation $\delta \mathbf{u}^{(k)}$ over the predictive horizon:

$$\tilde{\mathbf{u}}_t^{(k)} = \mathbf{u}_t + \delta \mathbf{u}^{(k)}, \quad \delta \mathbf{u}^{(k)} \sim \mathcal{N}(\mathbf{0}, \Sigma), \quad (14)$$

where $\delta \mathbf{u}^{(k)} \in \mathbb{R}^m$ is a trajectory-specific noise vector sampled once and applied uniformly over the entire prediction horizon.

For each sample k , the resulting latent trajectory $\{\tilde{\mathbf{z}}_t^{(k)}\}_{t=1}^T$ is decoded via pre-trained decoder ψ_θ to obtain the joint trajectory $\{\tilde{\mathbf{q}}_t^{(k)}\}_{t=1}^T$, from which the trajectory cost $S^{(k)}$ is evaluated in the operational space. Once all trajectory costs $\{S^{(k)}\}_{k=1}^K$ are evaluated, the importance weights $\{w^{(k)}\}_{k=1}^K$ are computed as in (7), and the optimal latent control sequence \mathbf{U}^* is updated as the importance-weighted average of the perturbed sequences, analogously to (8). Here, $\mathbf{U}^* = [\mathbf{u}_0^*, \mathbf{u}_1^*, \dots, \mathbf{u}_{T-1}^*]^T$ denotes the updated optimal latent control sequence corresponding to the sequence \mathbf{U} . The optimal latent state is then updated via first-order Euler integration, consistent with the latent dynamics defined in (10):

$$\mathbf{z}^* = \mathbf{z}_c + \mathbf{u}_0^* \Delta t, \quad (15)$$

where \mathbf{z}_c denotes the current latent state, propagated from the previous optimal solution. Finally, the optimal joint configuration is recovered by decoding \mathbf{z}^* as

$$\hat{\mathbf{q}}^* = \psi_\theta(\mathbf{z}^*), \quad (16)$$

where $\hat{\mathbf{q}}^*$ is the near-feasible configuration produced by the planning stage. The overall planning-stage procedure is summarized in Algorithm 1. Finally, $\hat{\mathbf{q}}^*$ is passed to the execution stage as a reference.

Algorithm 1 Planning Stage of the MC-MPPI Framework

Require:

- ψ_θ : Pre-trained decoder
 - \mathbf{z}_c : Current latent state
 - $\mathbf{U} = [\mathbf{u}_0, \dots, \mathbf{u}_{T-1}]$: Nominal control sequence
 - Σ : Noise covariance
 - K, T : Number of samples and horizon
- 1: **for** $k = 1, \dots, K$ **do** ▷ Parallel sampling
 - 2: $\delta \mathbf{u}^{(k)} \sim \mathcal{N}(\mathbf{0}, \Sigma)$ ▷ Single-instance sampling
 - 3: $\tilde{\mathbf{z}}_0^{(k)} \leftarrow \mathbf{z}_c$
 - 4: **for** $t = 0, \dots, T-1$ **do**
 - 5: $\tilde{\mathbf{u}}_t^{(k)} \leftarrow \mathbf{u}_t + \delta \mathbf{u}^{(k)}$
 - 6: $\tilde{\mathbf{z}}_{t+1}^{(k)} \leftarrow \tilde{\mathbf{z}}_t^{(k)} + \tilde{\mathbf{u}}_t^{(k)} \Delta t$
 - 7: $\tilde{\mathbf{q}}_{t+1}^{(k)} \leftarrow \psi_\theta(\tilde{\mathbf{z}}_{t+1}^{(k)})$ ▷ (13)
 - 8: **end for**
 - 9: Evaluate trajectory cost $S^{(k)}$ using $\{\tilde{\mathbf{z}}_t^{(k)}, \tilde{\mathbf{q}}_t^{(k)}\}_{t=1}^T$
 - 10: **end for**
 - 11: Compute importance weights $\{w^{(k)}\}_{k=1}^K$ via (7)
 - 12: $\mathbf{U}^* \leftarrow \sum_{k=1}^K w^{(k)} \tilde{\mathbf{U}}^{(k)}$ ▷ (8)
 - 13: $\mathbf{U} \leftarrow [\mathbf{u}_1^*, \dots, \mathbf{u}_{T-1}^*, \mathbf{0}]$
 - 14: $\mathbf{z}^* \leftarrow \mathbf{z}_c + \mathbf{u}_0^* \Delta t$ ▷ (15)
 - 15: $\hat{\mathbf{q}}^* \leftarrow \psi_\theta(\mathbf{z}^*)$ ▷ (16)
 - 16: **return** $\hat{\mathbf{q}}^*$
-

B. Execution Stage

Although the planning stage yields a near-feasible reference $\hat{\mathbf{q}}^*$, it does not lie exactly on \mathcal{M} due to approximation errors of the learned decoder, a phenomenon referred to as *manifold mismatch*. The execution stage therefore corrects this mismatch before passing the reference to the low-level controller.

To eliminate residual constraint violation while preserving task relevance, we formulate a single-step QP that finds the optimal next-state configuration \mathbf{q}^* on \mathcal{M} . Linearizing the closure constraint $\mathbf{h}(\mathbf{q}) = \mathbf{0}$ to first order around the current configuration \mathbf{q}_c yields the following formulation:

$$\begin{aligned} \hat{\mathbf{q}}^*, \mathbf{q}^* &= \arg \min_{\mathbf{q}, \dot{\mathbf{q}}} \|\dot{\mathbf{q}} - \dot{\mathbf{q}}_{\text{ref}}\|^2 + w_{\text{task}} \|\mathbf{J}_{\text{task}} \dot{\mathbf{q}} - \dot{\mathbf{x}}_{\text{task}}^*\|^2 \\ \text{s.t. } \mathbf{q} &= \mathbf{q}_c + \dot{\mathbf{q}} \Delta t, \\ \mathbf{J}_h \dot{\mathbf{q}} &= -\alpha \mathbf{h}(\mathbf{q}_c), \\ \dot{\mathbf{q}}_{\min} &\leq \dot{\mathbf{q}} \leq \dot{\mathbf{q}}_{\max}, \end{aligned} \quad (17)$$

where \mathbf{q}_c denotes the current joint configuration, $\mathbf{J}_h = \partial \mathbf{h} / \partial \mathbf{q}|_{\mathbf{q}_c}$ is the constraint Jacobian evaluated at \mathbf{q}_c , the reference velocity $\dot{\mathbf{q}}_{\text{ref}} = (\hat{\mathbf{q}}^* - \mathbf{q}_c) / \Delta t$ tracks the MC-MPPI solution, and the desired task velocity $\dot{\mathbf{x}}_{\text{task}}^* = -K_{p,\text{task}} \mathbf{e}_{\text{task}}(\mathbf{q}_c)$ regulates the operational-space error \mathbf{e}_{task} (e.g., the pose error of the tray center or the left end-effector) through the task Jacobian \mathbf{J}_{task} , weighted by w_{task} . The first equality relates the next configuration \mathbf{q}^* to \mathbf{q}_c via Euler integration, while the second drives the constraint residual $\mathbf{h}(\mathbf{q}_c)$ to zero at rate α . The velocity bounds $\dot{\mathbf{q}}_{\min} = (\mathbf{q}_{\text{lb}} - \mathbf{q}_c) / \Delta t$ and $\dot{\mathbf{q}}_{\max} = (\mathbf{q}_{\text{ub}} - \mathbf{q}_c) / \Delta t$ enforce the joint position limits.

Although $\hat{\mathbf{q}}^*$ is computed from near-feasible samples of the planning stage, the QP-based optimization in (17) may not preserve all of its task-relevant features, \mathbf{e}_{task} , because the

optimization direction toward \mathcal{M} is governed by the constraint Jacobian \mathbf{J}_h rather than the task objective. To address this, the task-tracking term explicitly biases the optimization toward the task-relevant region of \mathcal{M} , ensuring that the resulting configuration \mathbf{q}^* aligns with the actual task target.

The resulting \mathbf{q}^* is then passed to a low-level controller for execution on the robotic system.¹ In the rare event that the QP becomes infeasible, the framework employs a safe fallback strategy by maintaining the previous optimal configuration ($\mathbf{q}^* = \mathbf{q}_{\text{prev}}^*$) to ensure uninterrupted continuous operation.²

IV. EXPERIMENTS

This section validates the effectiveness of the proposed MC-MPPI framework through both simulation and real-world experiments. To this end, three main experiments are conducted. First, the framework is evaluated to validate its capability for handling constraints, demonstrating the essential role of the QP-based execution stage in resolving the manifold mismatch inherent in the learned VAE decoder. Second, the framework’s capability for static obstacle avoidance is evaluated, accompanied by an analysis of constant-innovation latent rollouts to characterize their effect on exploration efficiency and trajectory smoothness within the nonlinear latent space. Finally, the reactivity of MC-MPPI is assessed in an environment with dynamic obstacles. This final experiment is conducted on a real-world closed-chain dual-arm system, demonstrating both reactive capability and practical applicability.

A. Experiments Overview

To validate the proposed MC-MPPI framework on manifold-based equality constraints, a closed-chain dual-arm manipulation task is adopted as a representative benchmark. The system consists of two Panda manipulators (*Franka Emika Co.*) jointly grasping a flat tray, with configuration $\mathbf{q} \in \mathbb{R}^{14}$ subject to the equality constraint $\mathbf{h}(\mathbf{q}) = [\mathbf{h}_{\text{cc}}(\mathbf{q})^T, \mathbf{h}_{\text{flat}}(\mathbf{q})^T]^T \in \mathbb{R}^8$, comprising the following two terms.

The first is a 6-D closed-chain term that enforces the relative $SE(3)$ pose between the two end-effectors:

$$\mathbf{h}_{\text{cc}}(\mathbf{q}) = \log\left(\left({}^w\mathbf{T}_l {}^l\mathbf{T}_r^*\right)^{-1} {}^w\mathbf{T}_r\right) \in \mathbb{R}^6, \quad (18)$$

where ${}^w\mathbf{T}_l, {}^w\mathbf{T}_r \in SE(3)$ denote the left and right end-effector poses in the world frame, and ${}^l\mathbf{T}_r^*$ is the fixed relative transform required to maintain the bimanual grasp. The second is a 2-D tray flatness term enforcing zero roll and pitch about the tray center:

$$\mathbf{h}_{\text{flat}}(\mathbf{q}) = [\phi_{\text{tray}}, \theta_{\text{tray}}]^T = \mathbf{0} \in \mathbb{R}^2. \quad (19)$$

The resulting constraint manifold $\mathcal{M} = \{\mathbf{q} \in \mathbb{R}^{14} \mid \mathbf{h}(\mathbf{q}) = \mathbf{0}\}$ has an intrinsic dimension of $n - l = 6$, and the VAE is accordingly trained with a latent dimension of $m = 6$.

¹Note that the proposed framework is agnostic to the choice of low-level controller; in this work, a position controller is used in our closed-chain dual-arm implementation.

²It is worth noting that throughout all simulations and hardware experiments conducted in this study, the single-step QP consistently yielded a feasible solution, and this fallback condition was never triggered.

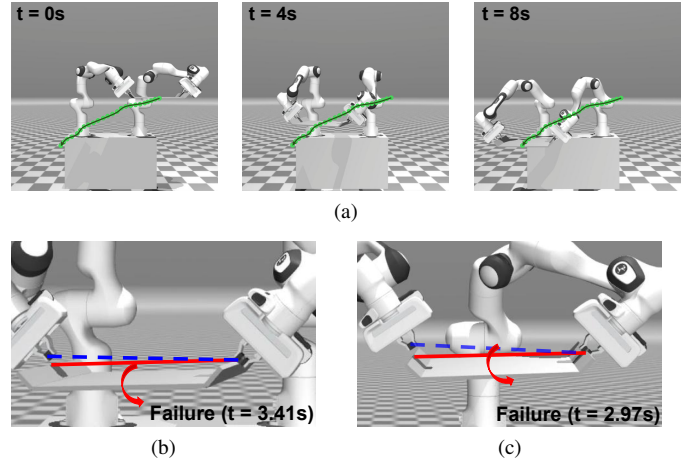


Fig. 2: Snapshots of the hard constraint validation experiment: (a) MC-MPPI successfully tracks the goal; (b) Latent MPPI fails at $t = 3.41$ s; (c) Vanilla MPPI fails at $t = 2.97$ s.

The experiments in Subsection IV-B and Subsection IV-C are conducted in MuJoCo [20], a high-fidelity physics simulator with full rigid-body dynamics and contact resolution. The MC-MPPI planner is configured with $K = 200$ samples, a prediction horizon of $T = 30$, and a control time step of $\Delta t = 0.01$ s across all experiments. Success is uniformly defined as preserving the bimanual grasp while driving both the position error below 0.01 m and the orientation error below 0.01 rad, a practical threshold that reflects the precision requirements of the closed-chain dual-arm task. The constraint violation is quantified as $\|\mathbf{h}(\mathbf{q})\|$, a mixed-unit norm combining position (m) and orientation (rad) terms. To execute these real-time control loops, all computations are performed on a computer equipped with an Intel Core i5-13400F CPU, 16 GB RAM, and an NVIDIA GeForce RTX 4060 Ti GPU.

During the MPPI planning stage, the trajectory cost S is evaluated as a weighted sum of five principal components:

$$S = S_{\text{track}} + S_{\text{coll}} + S_{\text{reg}} + S_{\text{limit}} + S_{\text{neutral}}, \quad (20)$$

where S_{track} penalizes the end-effector tracking error, S_{coll} ensures avoidance of both self-collisions and environmental obstacles, S_{reg} regularizes the latent control effort (i.e., the quadratic $\mathbf{u}^T \mathbf{R} \mathbf{u}$ penalty), S_{limit} enforces joint position boundaries alongside latent velocity limits, and S_{neutral} keeps the configuration close to a neutral joint posture to discourage drift toward kinematically awkward postures. Detailed formulations of these cost designs and the complete set of hyperparameters, as well as the VAE architecture, are available on the project website at <https://rcilab.github.io/mcmpi>

B. Validation of Hard Constraint Satisfaction

This experiment investigates the necessity of the QP-based execution stage by comparing the proposed MC-MPPI framework against two baselines: *Latent MPPI*, an ablated version of MC-MPPI that retains the VAE-based planning stage of Section III-A but omits the execution stage of Section III-B, and *Vanilla MPPI*, which performs standard MPPI of Section II directly in the joint configuration space with $\mathbf{u} = \dot{\mathbf{q}}$,

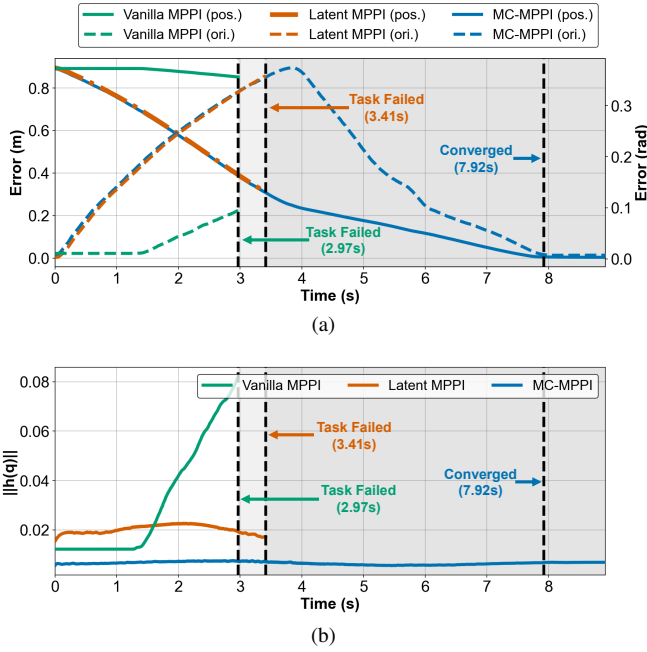


Fig. 3: Quantitative results of the hard constraint validation experiment: (a) tracking error and (b) equality-constraint violation.

where the equality constraint is treated through a large penalty cost on $\|h(q)\|$. The tray center is commanded to move from $(0.4, 0.4, 0.9)$ m to $(0.4, -0.4, 0.5)$ m, both with identity orientation. The standard deviation of the control perturbation $\delta u^{(k)}$ is uniformly set to 0.005 across all evaluated methods.

As shown in Figs. 2 and 3, MC-MPPI successfully converges to the target at 7.92 s while effectively satisfying the equality constraint $h(q)$ throughout the motion. The framework achieves this by maintaining the violation norm below the 0.01 threshold—yielding an average violation of 0.0066 ± 0.0007 —which reliably preserves both the closed-chain (h_{cc}) and tray flatness (h_{flat}) terms.

In contrast, both Vanilla MPPI and Latent MPPI fail before reaching the target, but their failure modes differ markedly. Vanilla MPPI fails earliest at 2.97 s, exhibiting an average violation of 0.0314 with a peak of 0.0820 while barely reducing the tracking error—reflecting the fundamental difficulty of finding feasible candidates in the ambient configuration space, where the soft penalty cannot constrain the chaotic exploration. Latent MPPI, by contrast, drives the tracking error down smoothly from the very first seconds, indicating that the VAE-learned latent space does enable meaningful exploration near the constraint manifold. However, despite this manifold-aware exploration, the residual manifold mismatch from the learned decoder—with an average violation of 0.0199 and a peak of 0.0226—accumulates over time and ultimately causes the bimanual grasp to break at 3.41 s.

Together, these results validate the two-stage design of MC-MPPI: the VAE-based planning stage successfully generates near-feasible trajectories that lie close to the constraint manifold—producing the smooth tracking behavior also observed in Latent MPPI—while the QP-based execution stage eliminates the residual manifold mismatch that Latent MPPI

cannot resolve, thereby enforcing constraint satisfaction in real-time execution.

C. Obstacle Avoidance under Static Environments

This experiment evaluates the proposed framework’s ability to navigate static obstacles while maintaining the manifold-based equality constraint. In addition, we examine the role of constant-innovation latent rollouts—originally introduced as single-instance sampling for task-space MPPI in [19]—when applied within the proposed VAE latent-space formulation, as shown in Fig. 4. While [19] established the benefit of this strategy in task space, its behavior in a learned latent space, where the decoder’s nonlinearity amplifies high-frequency components, has not been previously characterized. To empirically investigate this effect, we design a cluttered navigation scenario. Specifically, the tray center is commanded to move from $(0.4, 0.4, 0.9)$ m to $(0.4, -0.4, 0.5)$ m with identity orientation, while two spherical obstacles of radius 5 cm at $(0.4, 0.4, 0.6)$ m and $(0.4, -0.4, 0.7)$ m obstruct the direct path. The standard deviations of the latent control perturbations $\delta u^{(k)}$ and $\delta u_t^{(k)}$ are both set to 0.01 across all dimensions to enable sufficient exploration around the obstacles.

As shown in Figs. 4 and 5, the framework incorporating constant-innovation rollouts rapidly identifies a collision-free path and converges to the target at 7.60 s with an average constraint violation of 0.0069 ± 0.0003 . In contrast, the variant utilizing standard per-step sampling exhibits prolonged stagnation near the obstacles, requiring 79.25 s to converge with an average violation of 0.0067 ± 0.0010 . This disparity highlights a crucial characteristic of latent-space exploration: applying a constant control innovation across the prediction horizon allows the sampled trajectories to consistently explore deep along the constraint manifold in a specific direction. This sustained directional exploration is particularly critical under manifold-based equality constraints, where the feasible set is confined to a lower-dimensional subspace and admissible configurations near obstacles are extremely sparse.

Beyond exploration efficiency, maintaining a constant innovation in the latent space yields temporally smoother trajectories. Since the perturbation $\delta u^{(k)}$ acts as the latent velocity (14), holding it constant produces a smooth, linear latent trajectory. Without this property, per-step independent noise causes the latent velocity to fluctuate randomly. As hypothesized, the nonlinear nature of the VAE decoder ψ_θ heavily amplifies these high-frequency latent fluctuations, manifesting as jerky joint motions in the executed trajectory.³

D. Obstacle Avoidance under Dynamic Environments

This experiment evaluates the reactivity of MC-MPPI on the real closed-chain dual-arm hardware under time-varying environments. The bimanual system is commanded to transport a tray between uniformly sampled poses, where both the initial and goal configurations are drawn from $x \in [0.4, 0.6]$ m, $y \in [-0.3, 0.3]$ m, yaw $\in [-\pi/6, \pi/6]$, with $z \in [0.8, 1.0]$ m

³See the supplementary video on the project website.

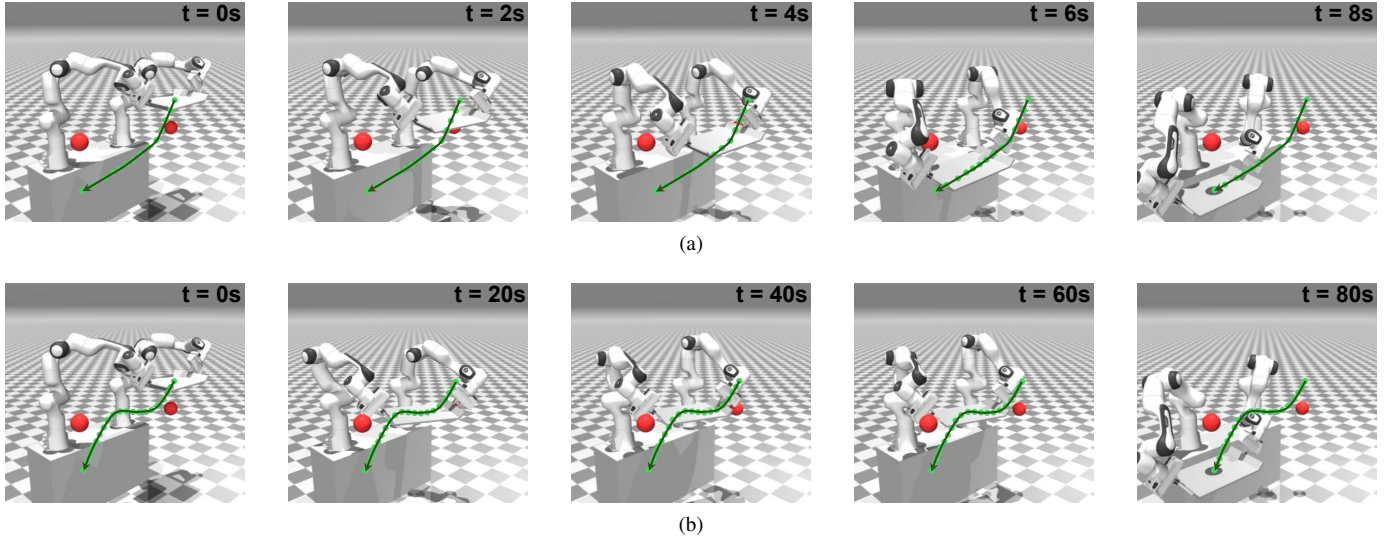


Fig. 4: Static obstacle avoidance performance under manifold constraints: (a) the proposed MC-MPPI with single-instance sampling with (14) successfully and efficiently navigates the cluttered environment; (b) the variant using standard per-step sampling exhibits prolonged stagnation.

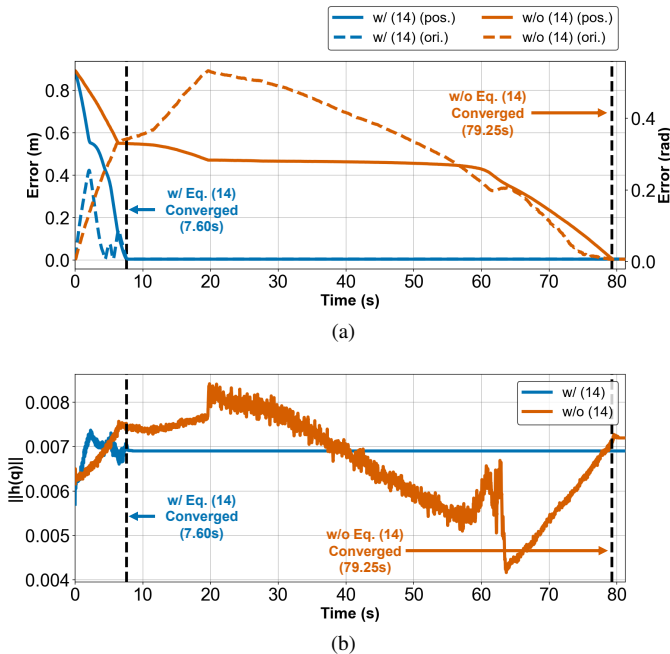


Fig. 5: Quantitative results of the static obstacle avoidance experiment comparing MC-MPPI with and without the constant-innovation strategy in (14): (a) tracking error and (b) equality constraint violation.

and $z \in [0.4, 0.6]$ m, respectively. During each trial, a single spherical obstacle of radius 5 cm traverses the workspace along either the x - or y -axis at a randomly selected speed of 0.1 or 0.2 m/s. A total of 40 trials are conducted under these randomized conditions.

Among the 40 trials, 38 are successfully completed, yielding a 95% success rate. As illustrated in Fig. 6, MC-MPPI successfully avoids the moving obstacle while maintaining an average constraint violation of 0.0067 ± 0.0010 , demonstrating that the decoupled two-stage architecture preserves constraint

enforcement even during aggressive evasion maneuvers. This reactivity is fundamentally enabled by the latent-space planning, which allows the receding-horizon controller to continuously adapt to unpredicted obstacle motion without requiring an explicit prediction model. As shown in Fig. 7 for a representative trial, the MPPI planning and QP execution stages run as parallel processes, with cycle times of 7.098 ± 0.729 ms (max 9.025 ms) and 1.277 ± 0.020 ms (max 1.369 ms), respectively, sustaining 100 Hz replanning and 500 Hz reference tracking throughout all trials. The two failure cases occur only when the obstacle moves rapidly along the x -axis, where insufficient lateral clearance within the dual-arm reachable region prevents successful evasion.

V. CONCLUSION

This paper presented Manifold-Constrained MPPI (MC-MPPI), a real-time sampling-based control framework that reliably maintains manifold-based equality constraints in real time. By decoupling the control problem into VAE-based latent space planning and QP-based execution-level correction, the framework successfully maintains hard-constraint satisfaction while preserving the derivative-free advantages of MPPI. Experimental results on a 14-DoF closed-chain dual-arm system demonstrated stable 100 Hz real-time performance and reliable constraint maintenance across both static and dynamic scenarios.

Building upon these results, our future research will focus on extending the framework's versatility and robustness. First, we aim to natively integrate inequality constraints—such as joint limits and obstacle avoidance—directly into the latent sampling paradigm, moving beyond the current cost-based soft penalty approach. Furthermore, we plan to adopt more advanced architectures, such as Conditional VAE (CVAE), to enhance the framework's generalization capabilities. This will allow a single model to adapt to diverse and parameterized constraint structures without the need for separate training,

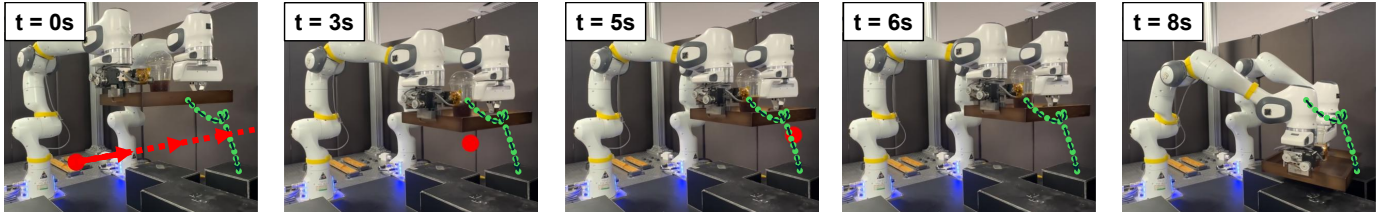


Fig. 6: Snapshots of the dynamic obstacle avoidance experiment for a representative trial on the real dual-arm system. A virtual moving sphere is introduced by feeding its trajectory directly into the controller, and the system successfully executes real-time evasion maneuvers while maintaining the manifold-based equality constraints.

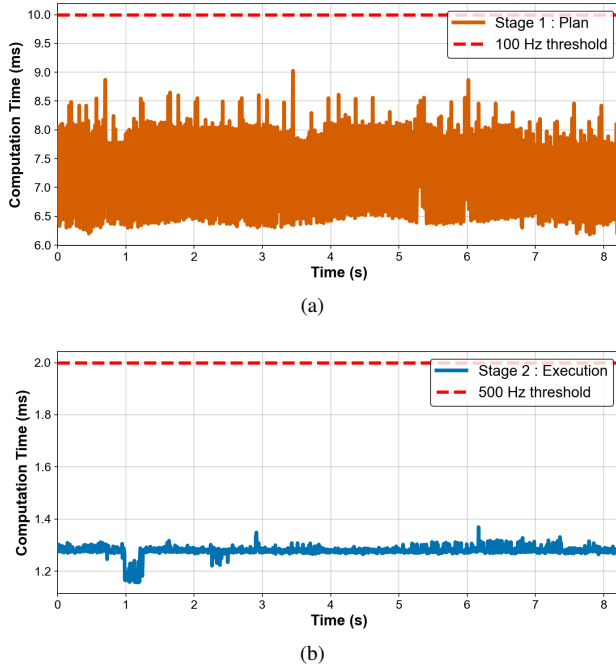


Fig. 7: Computation time of the dynamic obstacle avoidance experiment for a representative trial: (a) planning stage cycle time, consistently within the 10 ms budget (100 Hz); (b) execution stage cycle time, consistently within the 2 ms budget (500 Hz).

thereby broadening the practical applicability of the MC-MPPI framework to a wider range of constrained robotic tasks.

ACKNOWLEDGMENT

This research was supported by the National Research Foundation of Korea (NRF) grant funded by the Korea government (MSIT) (No. RS-2024-00411007), the National Research Council of Science & Technology (NST) grant funded by the Korea government (MSIT) (No. GTL25041-000), and the Korea Basic Science Institute (National Research Facilities and Equipment Center) grant funded by the Ministry of Science and ICT (No. RS-2025-00564593).

REFERENCES

- [1] H. Hu and J. Cao, "Practical tracking control for dual-arm robot with output constraints," *International Journal of Control, Automation and Systems*, vol. 20, no. 10, pp. 3264–3273, 2022.
- [2] J. Schulman, Y. Duan, J. Ho, A. Lee, I. Awwal, H. Bradlow, J. Pan, S. Patil, K. Goldberg, and P. Abbeel, "Motion planning with sequential convex optimization and convex collision checking," *The International Journal of Robotics Research*, vol. 33, no. 9, pp. 1251–1270, 2014.
- [3] J. Fliege and A. I. F. Vaz, "A method for constrained multiobjective optimization based on sqp techniques," *SIAM Journal on Optimization*, vol. 26, no. 4, pp. 2091–2119, 2016.
- [4] Y. Tassa, N. Mansard, and E. Todorov, "Control-limited differential dynamic programming," in *2014 IEEE International Conference on Robotics and Automation (ICRA)*. IEEE, 2014, pp. 1168–1175.
- [5] Z. Xie, C. K. Liu, and K. Hauser, "Differential dynamic programming with nonlinear constraints," in *2017 IEEE International Conference on Robotics and Automation (ICRA)*. IEEE, 2017, pp. 695–702.
- [6] W. Li and E. Todorov, "Iterative linear quadratic regulator design for nonlinear biological movement systems," in *First International Conference on Informatics in Control, Automation and Robotics*, vol. 2. SciTePress, 2004, pp. 222–229.
- [7] G. Williams, A. Aldrich, and E. A. Theodorou, "Model predictive path integral control: From theory to parallel computation," *Journal of Guidance, Control, and Dynamics*, vol. 40, no. 2, pp. 344–357, 2017.
- [8] G. Williams, P. Drews, B. Goldfain, J. M. Rehg, and E. A. Theodorou, "Aggressive driving with model predictive path integral control," in *2016 IEEE international conference on robotics and automation (ICRA)*. IEEE, 2016, pp. 1433–1440.
- [9] M. Bhardwaj, B. Sundaralingam, A. Mousavian, N. D. Ratliff, D. Fox, F. Ramos, and B. Boots, "Storm: An integrated framework for fast joint-space model-predictive control for reactive manipulation," in *Conference on Robot Learning*. PMLR, 2022, pp. 750–759.
- [10] I. Ardiyanto, M. I. Solihin, and H. A. Nugroho, "Sampling-based safety-critical control for planar quadrotors with suspended payloads," *International Journal of Control, Automation and Systems*, vol. 23, no. 10, pp. 3115–3125, 2025.
- [11] J. Yin, C. Dawson, C. Fan, and P. Tsiotras, "Shield model predictive path integral: A computationally efficient robust mpc method using control barrier functions," *IEEE Robotics and Automation Letters*, vol. 8, no. 11, pp. 7106–7113, 2023.
- [12] E. M. Andrejev, A. Manoharan, K.-E. Unt, and A. K. Singh, " π -mppi: a projection-based model predictive path integral scheme for smooth optimal control of fixed-wing aerial vehicles," *IEEE Robotics and Automation Letters*, 2025.
- [13] T. Miura, N. Akai, K. Honda, and S. Hara, "Spline-interpolated model predictive path integral control with stein variational inference for reactive navigation," in *2024 IEEE International Conference on Robotics and Automation (ICRA)*. IEEE, 2024, pp. 13 171–13 177.
- [14] L. Park, K. Jang, and S. Kim, "Csc-mppi: A novel constrained mppi framework with dbscan for reliable obstacle avoidance," in *2025 IEEE/RSJ International Conference on Intelligent Robots and Systems (IROS)*. IEEE, 2025, pp. 19 645–19 652.
- [15] G. Sutanto, I. R. Fernández, P. Englert, R. K. Ramachandran, and G. Sukhatme, "Learning equality constraints for motion planning on manifolds," in *Conference on Robot Learning*. PMLR, 2021, pp. 2292–2305.
- [16] C. Acar and K. P. Tee, "Approximating constraint manifolds using generative models for sampling-based constrained motion planning," in *2021 IEEE International Conference on Robotics and Automation (ICRA)*. IEEE, 2021, pp. 8451–8457.
- [17] D. P. Kingma and M. Welling, "Auto-encoding variational bayes," in *Proceedings of the International Conference on Learning Representations (ICLR)*, 2014.
- [18] S. Kim, K. Jang, S. Park, Y. Lee, S. Y. Lee, and J. Park, "Continuous task transition approach for robot controller based on hierarchical quadratic

- programming,” *IEEE Robotics and Automation Letters*, vol. 4, no. 2, pp. 1603–1610, 2019.
- [19] D. Kim, E. Im, Y. Kim, M. Lim, and Y. Lee, “Single-instance sampling for computationally efficient and accurate real-time task space mppi control,” *IEEE Transactions on Robotics*, vol. 41, pp. 6327–6344, 2025.
- [20] E. Todorov, T. Erez, and Y. Tassa, “Mujoco: A physics engine for model-based control,” in *2012 IEEE/RSJ international conference on intelligent robots and systems*. IEEE, 2012, pp. 5026–5033.